15th Triennial World Congress, Barcelona, Spain

INSTABILITY MECHANISMS IN INDIRECT FIELD ORIENTED CONTROL DRIVES: THEORY AND EXPERIMENTAL RESULTS

A. S. Bazanella R. Reginatto *

* *Department of Electrical Engineering, Universidade Federal do Rio Grande do Sul, Av. Osvaldo Aranha 103, 90035-190, Porto Alegre, RS, Brazil, e-mail: bazanela@eletro.ufrgs.br*

Abstract: Analysis of saddle-node and Hopf bifurcations in IFOC drives due to errors in the estimate of the rotor time constant is presented. Experimental results showing such bifurcations are given and guidelines for drive commissioning are derived from these results.

Keywords: Indirect field oriented control; induction motors; bifurcations

1. INTRODUCTION

The commissioning of an indirect field oriented control (IFOC) drive requires the knowledge of the rotor time constant, a parameter that can vary widely in practice (Krishnan and Doran, 1987; Marino *et al.*, 1993) and is known to cause performance and stability problems. It has been shown that the speed control of induction motors through IFOC is globally asymptotically stable for any constant load torque if the rotor time constant is perfectly known or the error in its estimation is sufficiently small (De Wit *et al.*, 1996; Bazanella and Reginatto, 2000). In a previous paper (Bazanella and Reginatto, 2000) we also showed that saddle-node bifurcations occur for certain values of the mismatch in this estimation and certain load conditions. Another possible mechanism for loss of stability, namely, the occurrence of Hopf bifurcations, has been considered in (Bazanella and Reginatto, 2001; Bazanella *et al.*, 1999; De Wit *et al.*, 1996; Espinosa-Perez *et al.*, 1998). Contrary to saddle-node bifurcations, this mechanism of loss of stability depends on the settings of the speed control loop (De Wit *et al.*, 1996; Espinosa-Perez *et al.*, 1998; Bazanella *et al.*, 1999). In the recent works (Reginatto and Bazanella, 2000; Bazanella *et al.*, 2000), effective results have been provided to analyze the global asymptotic stability property of IFOC drives. Also in this case, the setting of the PI speed loop controller plays a fundamental role on the size of the region on the parameter space where the IFOC drives exhibits this important property.

This set of results elucidates the influence of all relevant tunable parameters in an IFOC drive on its stability properties. In this paper we provide experimental results that confirm and further clarify these theoretical findings. On the base of these results, we provide useful guidelines for the setting of the tunable parameters in the commissioning of an IFOC drive. The guidelines are intended for a design that keeps all possible instability mechanisms far enough from a practical operating region in the parameter space.

The paper is organized as follows. In Section 2 the system modeling and the control equations are given and some additional convenient notation and concepts are introduced. Analysis and experimental verification of saddle-node bifurcations are presented in Section 3. Results regarding Hopf bifurcations are presented in Section 4. Based on these results, in Section 5 we derive guidelines for setting the estimate of the rotor time constant and the parameters of the PI speed controller in order to guarantee stability of the system for practical parameter mismatches.

2. PRELIMINARIES

2.1 *System modeling*

We consider the indirect field oriented control (IFOC) of induction motor drives. Field oriented control is usually employed as a means to achieve high performance transient response in speed, position, or torque control. The implementation of IFOC employs stator current control, i.e., the induction machine is current fed, and allows three control inputs, namely: i_{ds}, the direct axis stator current component; i_{qs}, the quadrature axis stator current component; and ω_{sl}, the slip frequency (Novotny and Lorenz, 1986; Leonhard, 1985).

IFOC consists in setting ω_{sl} and a specific initialization procedure in the attempt to achieve a control decoupling between i_{ds} and i_{qs}, the first acting on the rotor flux level, while the later acting on the developed torque. More specifically, we have (Novotny and Lorenz, 1986; De Wit *et al.*, 1996):

$$\omega_{sl} = \hat{c}_1 \frac{i_{qs}}{i_{ds}} \tag{1}$$

$$i_{ds} = u_2^0 \tag{2}$$

where $\hat{c}_1$ is an estimate for the inverse rotor time constant $c_1 = \frac{R_r}{L_r}$, L_r being the rotor inductance and R_r the rotor resistance, and u_2^0 is some constant which defines the rotor flux level.

In speed regulation applications, usually a PI regulator is used to act on the remaining control input i_{qs},

$$i_{qs} = k_p e_w + k_i \int_0^t e_w(\zeta)\, d\zeta \tag{3}$$

where k_p and k_i are the gains of the PI speed controller and $e_w = w_{ref} - w$ is the rotor speed error.

If $\hat{c}_1 = c_1$, that is, if we have a perfect estimate of the rotor time constant, we say that the control is tuned, otherwise it is said to be detuned. Accordingly, we define

$$\kappa \triangleq \frac{\hat{c}_1}{c_1} \tag{4}$$

as the degree of tuning. It is clear that $\kappa > 0$ and the control is tuned if and only if $\kappa = 1$.

By choosing state variables $[x_1,\, x_2,\, x_3,\, x_4] = [\lambda_{qr},\, \lambda_{dr},\, e_w,\, i_{qs}]$, we obtain the induction motor model under field oriented control (1)-(2) and PI speed regulation (3) described as:

$$\dot{x}_1 = -c_1 x_1 + c_2 x_4 - \frac{\kappa c_1}{u_2^0} x_2 x_4 \tag{5}$$

$$\dot{x}_2 = -c_1 x_2 + c_2 u_2^0 + \frac{\kappa c_1}{u_2^0} x_1 x_4 \tag{6}$$

$$\dot{x}_3 = -c_3 x_3 - c_4[c_5(x_2 x_4 - u_2^0 x_1) - T_e] \tag{7}$$

$$\dot{x}_4 = k_c x_3 - k_p c_4[c_5(x_2 x_4 - u_2^0 x_1) - T_e] \tag{8}$$

where λ_{qr} and λ_{dr} stand for the quadrature and direct axis components of the rotor flux; T_m is the load torque, which is assumed constant; c_1 to c_5 are machine parameters; and we have defined $k_c \triangleq k_i - k_p c_3$ and $T_e \triangleq T_m + \frac{c_3}{c_4} w_{ref}$.

It is easy to show that for position regulation with a proportional-derivative controller the same model is obtained after a change of variables, so that all the results derived for speed regulation are also valid for position regulation.

2.2 *The tuned system*

A constant rotor flux must be established inside the motor before the system can be operated. This is called the magnetization phase of IFOC, and is achieved by setting $i_{ds} = u_2^0$ and $w_{ref} = 0$ with the motor in standstill condition. The steady-state reached under these conditions is given by $x = x^o = [0,\, \frac{c_2}{c_1} u_2^0,\, 0,\, 0]'$, which is considered the initial state for IFOC operation.

In the tuned case, $\kappa = 1$, the model (5)-(8) simplifies considerably. First, notice that starting from $x(0) = x^o$, the fluxes x_1 and x_2 remain constant for all times, regardless of the behavior of x_4. Now, taking this into account, the remaining equations (7)-(8) can be rearranged as

$$\begin{bmatrix} \dot{x}_3 \\ \dot{x}_4 \end{bmatrix} = \begin{bmatrix} -c_3 & -\dfrac{c_4 c_5 c_2 u_2^0}{c_1} \\ (k_i - k_p c_3) & -\dfrac{k_p c_4 c_5 c_2 u_2^0}{c_1} \end{bmatrix} \begin{bmatrix} x_3 \\ x_4 \end{bmatrix} + \begin{bmatrix} c_3 & c_4 \\ k_p c_3 & k_p c_4 \end{bmatrix} \begin{bmatrix} w_{ref} \\ T_m \end{bmatrix} \tag{9}$$

which is a second-order *linear* system. We shall refer to the dynamic system (9) as the *tuned system*, which is usually taken as a base for setting the PI gains.

The tuned system just defined represents an ideal situation, in which perfect field-orientation is achieved. Under this condition optimal performance can be achieved, and the PI speed controller is set for the desired performance. Since in this case the controlled system is linear and of order two, the tuning of the PI controller under the assumption of perfect field-orientation is simple, and in theory arbitrary performance can be achieved.

From (9), the closed-loop eigenvalues are the roots of the characteristic polynomial

$$p_T(\lambda) = \lambda^2 + (c_3 + k_p K)\lambda + k_i K \tag{10}$$

where $K \triangleq \frac{c_2 c_4 c_5 u_2^0}{c_1}$. Then the PI parameters k_p and k_i can be chosen to arbitrarily assign the closed-loop

eigenvalues of the tuned system. Indeed, let the desired closed-loop characteristic (Hurwitz) polynomial be written as

$$\lambda^2 + a_1\lambda + a_0, \quad a_0 > 0,\ a_1 > 0 \tag{11}$$

Then, equating the coefficients in (10) and (11) yields

$$k_p = \frac{a_1 - c_3}{K}, \quad k_i = \frac{a_0}{K} \tag{12}$$

Once the closed-loop poles are chosen the parameters k_p and k_i can be calculated from (12).

3. SADDLE-NODE BIFURCATION

3.1 *Analysis*

Let us define the dimensionless variables $r \triangleq \frac{x_4^e}{u_2^0}$ and $r^* \triangleq \frac{T_e c_1}{c_5 c_2 (u_2^0)^2}$. The constant r^* represents the system loading, since it is proportional to the electrical torque developed in steady-state. The parameter r can be shown to satisfy the third-order polynomial equation (Bazanella and Reginatto, 2000)

$$\kappa r^3 - r^* \kappa^2 r^2 + \kappa r - r^* = 0 \tag{13}$$

and the equilibria can be written as

$$\begin{bmatrix} x_1^e \\ x_2^e \\ x_3^e \\ x_4^e \end{bmatrix} = \begin{bmatrix} \frac{c_2 u_2^0}{c_1} \frac{1-\kappa}{1+\kappa^2 r^2} r \\ \frac{c_2 u_2^0}{c_1} \frac{1+\kappa r^2}{1+\kappa^2 r^2} \\ 0 \\ u_2^0\, r \end{bmatrix} \tag{14}$$

The complete characterization of the equilibria, as given by the polynomial equation (13), is illustrated in Figure 2 (Bazanella and Reginatto, 2000). The two curves, on the (κ, r^*) parameter space, delimit the region where equation (13) has 3 real solutions (3 equilibrium points). For any point outside the region we have a unique equilibrium point. The point where the two curves intersect is $\kappa = 3$, $r^* = \frac{\sqrt{3}}{3}$. Thus, we have a unique equilibrium point for any load condition if and only if $\kappa < 3$.

If the load and/or the degree of tuning are modified gradually starting from the tuned condition, then a saddle-node bifurcation occurs when one of the lines in figure 2 is crossed. The branching diagram for $\kappa = 4$ is presented in Figure 3. If the load is increased gradually, when the saddle-node bifurcation is reached a jump will occur in current, bringing it to another equilibrium where the current level is more than five times larger.

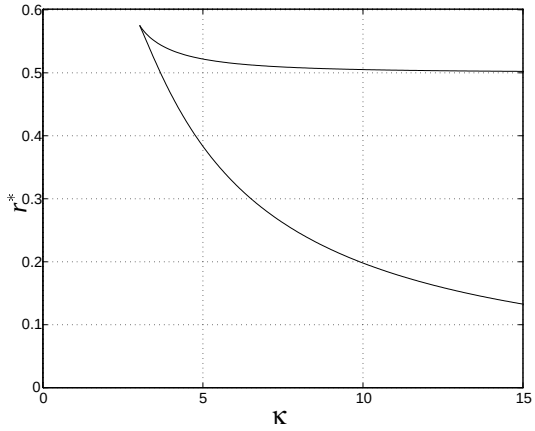

Fig. 1. Locus of the points in the parameter space where the number of equilibria changes.

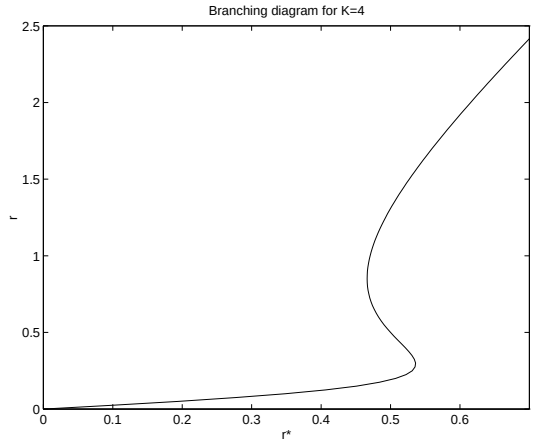

Fig. 2. Branching diagram for $\kappa = 4$.

Table 1. Motor data.

Rated power	$\frac{1}{3}$ hp
Rated frequency	60 Hz
Rated voltage	380 V
Rated current	0.8 A
c_1	50 s^{-1}
c_2	25 Ω
c_3	0.54 s^{-1}
c_4	714 $kg^{-1}m^{-2}$
c_5	2.84

3.2 *Experimental results*

Experimental results are obtained in a current-fed IFOC drive with a DC generator providing the load. By varying the electrical load of the DC generator the mechanical load of the drive is varied, always getting a load torque proportional to the drive speed. Data for the experimental setting are given in Table 1

A saddle-node bifurcation for $\kappa \approx 4$ can be observed in the experimental results shown in figures 4-5. We can not guarantee the exact value of κ because we don't have a perfect estimate of c_1 for this operating condition. The field current and load of the DC generator are set at a constant level such that the steady-state electrical torque and therefore the equivalent load r^*

are significantly increased by increasing the reference speed. The direct axis current is set at $u_2^0 = 0.4\,A$.

As the reference speed is increased, the equivalent load r^* also increases, eventually reaching the point where a jump in current occurs, at $t = 4\ s$. Since the final value of the current is much above nominal, motor protection is activated, current drops to zero and the motor goes to stall. It can be seen in figure 4 that the current specified by the speed controller does jump, although the actual current tends to zero due to actuation of the protection.

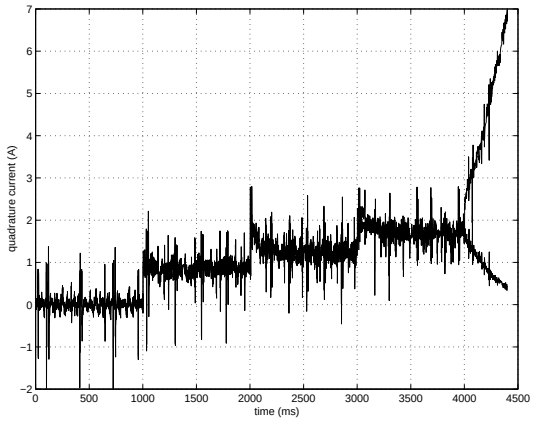

Fig. 3. Speed reference steps until saddle-node bifurcation: reference and measured quadrature current.

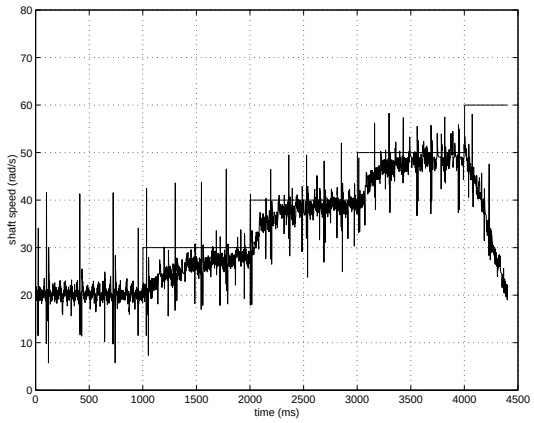

Fig. 4. Speed reference steps until saddle-node bifurcation: reference and measured speed.

We also provide results with $\kappa \approx 1$ in figures 6-7. It can be seen that the jump for $\kappa \approx 4$ has occurred at the last step of reference speed. The average value of the quadrature current in this operating condition for $\kappa \approx 1$ is measured as $i_q = 0.166\,A$, which corresponds to $r^* = 0.415$. The jump is observed before the bifurcation actually occurs, at a point where the lower equilibrium point in the branching diagram in Figure 3 still exists but its region of attraction is very small.

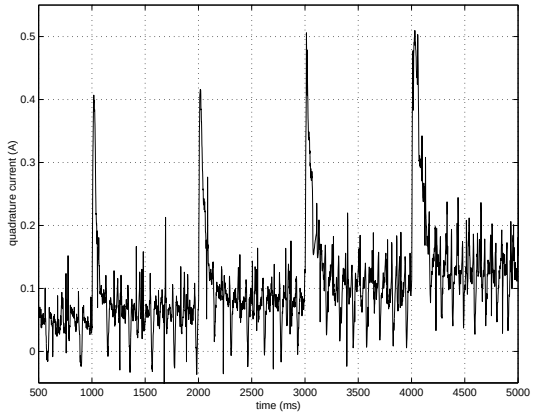

Fig. 5. Speed reference steps in the "tuned" condition: measured quadrature current.

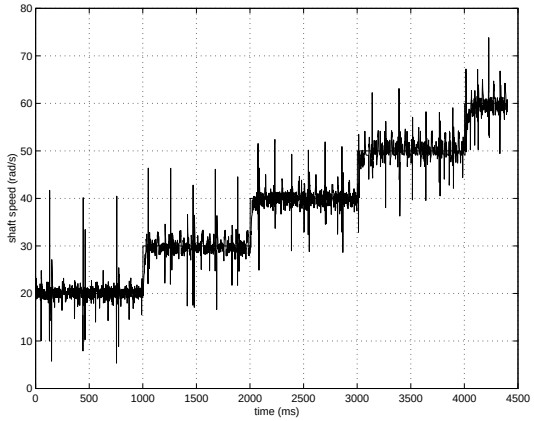

Fig. 6. Speed reference steps in the "tuned" condition: reference and measured speed.

4. HOPF BIFURCATIONS

4.1 *Analysis*

A Hopf bifurcation characterizes an equilibrium becoming unstable by the crossing of the $j\omega$ axis by two complex conjugate eigenvalues of the jacobian. In the important case of zero load operation, a closed form condition for existence of Hopf bifurcations can be derived as follows (Bazanella *et al.*, 1999; Bazanella and Reginatto, 2001).

Lemma 1. Let $c_3 \equiv 0$ and $T_m \equiv 0$. Then, no Hopf bifurcation takes place for any $\kappa > 0$ provided that a_0, a_1 satisfy the relation

$$a_0 \leq a_1(c_1 + a_1) \tag{15}$$

If condition 15 is not satisfied, then a Hopf bifurcation takes place at

$$\kappa = \kappa_h \stackrel{\Delta}{=} \frac{a_0(c_1 + a_1)}{c_1(a_0 - a_1(c_1 + a_1))} \tag{16}$$

$\diamond$

Condition (15) is satisfied whenever the closed-loop eigenvalues for the tuned system are chosen to be

real. If complex closed-loop eigenvalues are desired, then the imaginary part has to be chosen sufficiently small in order to satisfy (15). Figure 8 illustrates the situation for the complex eigenvalues case, i.e., $\lambda_{1,2} = -\sigma \pm j\omega$. The value of κ_h is plotted as a function of σ/c_1 and $j\omega/c_1$, the normalized real and imaginary part of the chosen eigenvalues for the tuned system, respectively. The figure also shows the region, in the $(\sigma, j\omega)$ plane, where no Hopf bifurcation takes place for any κ. We can see that κ_h approaches ∞ at the boundary of that region and rapidly decreases to practical values as the damping is decreased.

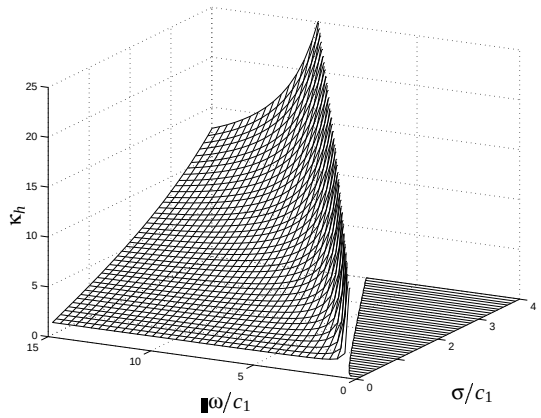

Fig. 7. Parameter chart for the zero load case. Tuned system eigenvalues $\lambda_{1,2} = -\sigma \pm j\omega$. The dashed region in the $(\sigma, j\omega)$ plane illustrates the region where no Hopf bifurcation takes place for any κ.

4.2 *Experimental results*

Experimental results are provided for a given setting of the speed loop. The PI controller is set as $k_p = 4.7E-3\,As$ and $k_i = 0.1\,A$. Several experiments have been performed under no load, with different values of κ. Typical results are given in Figures 9-12.

Figures 9-10 show the result for $\kappa \approx 3$ whereas the behavior at the "tuned" condition ($\kappa \approx 1$) is presented in figures 11-12. It can be observed that this PI tuning, for which the response of the tuned system is fast and oscillatory, results in a Hopf bifurcation for $\kappa = 3$, which agrees with the theoretical analysis.

5. SETTING OF THE PI GAINS

It is reasonable to think of a PI setting that would avoid Hopf bifurcations to take place for $\kappa \in (0,\ 3]$. We cannot pursue anything larger than that, since for $\kappa > 3$ there always exist a range for r^* for which an unstable equilibrium point exists, regardless of the PI settings (see Figure 2). On the other hand, it is advisable to keep bifurcations far enough in order to avoid unsatisfactory transient behavior.

In analyzing the occurrence of Hopf bifurcation, we also have to consider the effect of the normalized load

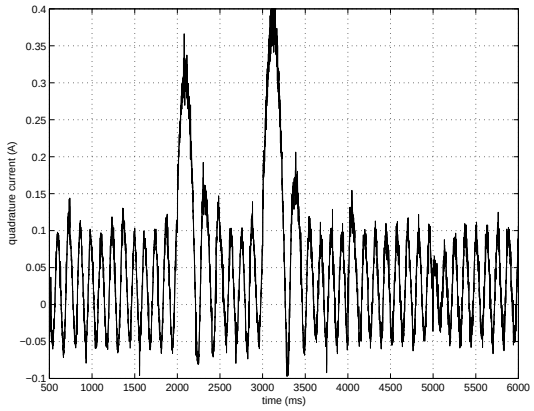

Fig. 8. Speed reference steps until Hopf bifurcation: measured quadrature current.

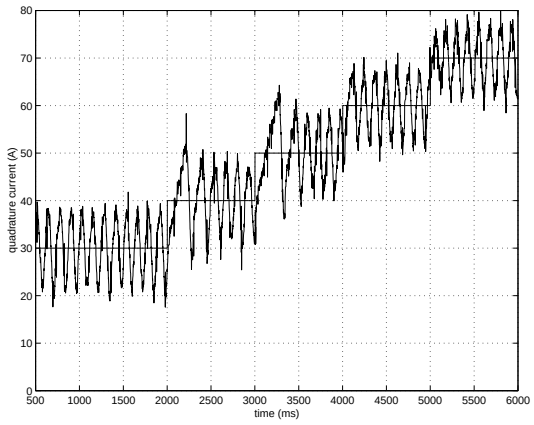

Fig. 9. Speed reference steps until Hopf bifurcation: reference and measured speed.

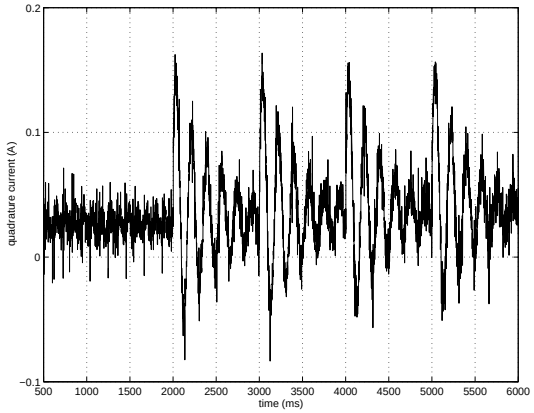

Fig. 10. Speed reference steps in the "tuned" condition: measured quadrature current.

r^*. It is simple to verify that r^* coincides with the ratio x_4^e/u_2^0 for tuned operation. In general, this ratio is no larger than 2, so we concentrate on a range for r^* given by $0 \leq r^* \leq 2$. This includes the zero load operation for which experimental results have been provided.

Following the statement of Lemma 1 (see Fig. 8), Hopf bifurcations can be avoided by setting the PI gains so that the closed-loop poles of the tuned system are real or with high damping. Results presented in (Bazanella *et al.*, 1999) also show that

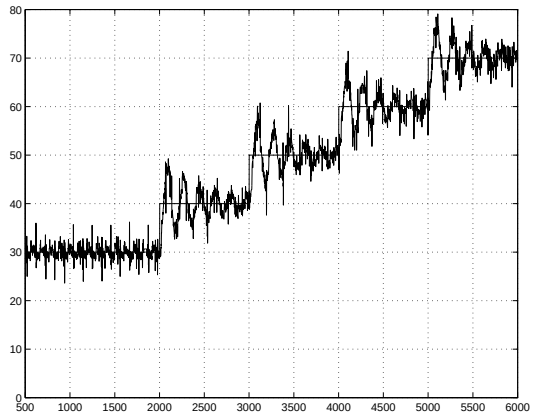

Fig. 11. Speed reference steps in the ”tuned” condition: reference and measured speed.

these poles should not be farther left in the complex plane than $-23c_1$, a result that is also consistent with the robustness of global asymptotic stability provided in (Reginatto and Bazanella, 2000). Thus, poor PI setting can cause Hopf bifurcations basically in two different ways. One is to make the closed-loop response oscillatory by assigning complex conjugate eigenvalues with low damping. The second one is to force the closed-loop response to be very fast by choosing the closed-loop eigenvalues too far away to the left in the complex plane.

Based on this analysis we can propose as a guideline for setting the PI gains the following: chose real closed-loop poles for the tuned system such that the desired transient performance is achieved, but always avoiding to make the poles larger than $10c_1$ in order to keep the bifurcation far away, thus improving robustness.

6. REFERENCES

Bazanella, A. S. and R. Reginatto (2001). Robust tuning of the speed loop in indirect field oriented control of induction motors. *Automatica* **37**(11), 1811–1818.

Bazanella, A. S., R. Reginatto and R. Valiatti (2000). Robustness margins for global asymptotic stability in indirect field-oriented control of induction motors. In: *XIII Congresso Brasileiro de Automática*. Florianópolis, Brasil. pp. 1048–1053.

Bazanella, A.S. and R. Reginatto (2000). Robustness margins for indirect field oriented control of induction motors. *IEEE Trans. Aut. Cont.* **45**(6), 1226–1231.

Bazanella, A.S., R. Reginatto and R. Valiati (1999). On hopf bifurcations in indirect field oriented control of induction motors: designing a robust PI controller. In: *Conference on Decision and Control*. Phoenix, Arizona.

De Wit, P.A.S., R. Ortega and I. Mareels (1996). Indirect field-oriented control of induction motors is robustly globally stable. *Automatica* **32**(10), 1393–1402.

Espinosa-Perez, G., G. Chang, R. Ortega and E. Mendes (1998). On field-oriented control of induction motors: Tuning of the PI gains for performance enhancement. In: *Conference on Decision and Control*. Tampa, Florida. pp. WM15–2.

Krishnan, R. and F. C. Doran (1987). Study of parameter sensitivity in high-performance inverter-fed induction motor drive systems. *IEEE Trans. Ind. Applic.* **IA-23**(4), 623–635.

Leonhard, W. (1985). *Control of Electrical Drives*. Springer-Verlag. Berlin.

Marino, R., S. Peresada and P. Valigi (1993). Adaptive input-output linearizing control of induction motor. *IEEE Trans. Aut. Cont.* **38**(2), 208–221.

Novotny, D.W. and R.D. Lorenz (1986). *Introduction to Field Orientation and High Performance AC Drives*. IEEE.

Reginatto, R. and A. S. Bazanella (2000). Robustness of global asymptotic stability in indirect field-oriented control of induction motors. In: *Conference on Decision and Control*. Sydney, Australia.